Journal of
MEDICAL GENETICS

ADAP2 in heart development: a candidate gene for the occurrence of Cardiovascular Malformations in NF1 Microdeletion Syndrome

Journal:	*Journal of Medical Genetics*
Manuscript ID:	jmedgenet-2013-102240.R1
Article Type:	Original Article
Date Submitted by the Author:	n/a
Complete List of Authors:	Venturin, Marco; Dipartimento di Biotecnologie Mediche e Medicina Traslazionale, Università degli studi di Milano, Carra, Silvia; Dipartimento di Bioscienze, Università degli studi di Milano, Gaudenzi, Germano; Dipartimento di Bioscienze, Università degli studi di Milano, Brunelli, Silvia; Dipartimento di Scienze della Salute, Università degli Studi di Milano-Bicocca, Gallo, Guido; Dipartimento di Bioscienze, Università degli studi di Milano, Moncini, Silvia; Dipartimento di Biotecnologie Mediche e Medicina Traslazionale, Università degli studi di Milano, Cotelli, Franco; Dipartimento di Bioscienze, Università degli studi di Milano, Riva, Paola; Dipartimento di Biotecnologie Mediche e Medicina Traslazionale, Università degli studi di Milano,
Keywords:	Molecular genetics, Congenital heart disease

Title

***ADAP2* in heart development: a candidate gene for the occurrence of Cardiovascular Malformations in NF1 Microdeletion Syndrome**

[*]Marco Venturin[1], [*]Silvia Carra[2], [*]Germano Gaudenzi[2], Silvia Brunelli[3], Guido Roberto Gallo[2], Silvia Moncini[1], [#]Franco Cotelli[2], [#]Paola Riva[1]

[1] Dipartimento di Biotecnologie Mediche e Medicina Traslazionale, Università degli Studi di Milano, Milan, Italy

[2] Dipartimento di Bioscienze, Università degli Studi di Milano, Milan, Italy

[3] Dipartimento di Scienze della Salute, Università degli Studi di Milano-Bicocca, Monza (MB), Italy

[*] These authors equally contributed to the work

[#] These authors equally contributed to the work

Key Words

NF1 Microdeletion Syndrome, Cardiovascular Malformations, *ADAP2*, Heart Development, Zebrafish

Word Count

3980

Corresponding Authors

Marco Venturin, Ph.D.
Dipartimento di Biotecnologie Mediche e Medicina Traslazionale, Università degli Studi di Milano;
Via Viotti 3/5, 20133 Milan, Italy;

Tel. +39 02 50315841;
Fax. +39 02 50315864;
E-mail: marco.venturin@unimi.it

Paola Riva, Ph.D.
Dipartimento di Biotecnologie Mediche e Medicina Traslazionale, Università degli Studi di Milano;
Via Viotti 3/5, 20133 Milan, Italy;
Tel. +39 02 50315862;
Fax. +39 02 50315864;
E-mail: paola.riva@unimi.it

ABSTRACT

Background

Cardiovascular malformations have a higher incidence in patients with NF1 microdeletion syndrome compared to NF1 patients with intragenic mutation, presumably owing to haploinsufficiency of one or more genes included in the deletion interval and involved in heart development. In order to identify which genes could be responsible for cardiovascular malformations in the deleted patients, we carried out expression studies in mouse embryos and functional studies in zebrafish.

Methods and results

The expression analysis of three candidate genes included in the NF1 deletion interval, *ADAP2*, *SUZ12* and *UTP6*, performed by *in situ* hybridization, showed the expression of *ADAP2* murine ortholog in heart during fundamental phases of cardiac morphogenesis.

In order to investigate the role of *ADAP2* in cardiac development, we performed loss-of-function experiments of zebrafish *ADAP2* ortholog, *adap2*, by injecting two different morpholino oligos (*adap2*-MO and UTR-*adap2*-MO). *adap2*-MOs injected embryos (morphants) displayed *in vivo* circulatory and heart shape defects. The molecular characterization of morphants with cardiac specific markers showed that the injection of *adap2*-MOs causes defects in heart jogging and looping. In addition, morphological and molecular analysis of *adap2* morphants demonstrated that the loss of *adap2* function leads to defective valvulogenesis, suggesting a correlation between *ADAP2* haploinsufficiency and the occurrence of valve defects in NF1-microdeleted patients.

Conclusions

Overall, our findings indicate that *ADAP2* has a role in heart development and might be a reliable candidate gene for the occurrence of cardiovascular malformations in patients with NF1 microdeletion and, more generally, for the occurrence of a subset of congenital heart defects.

INTRODUCTION

NF1 microdeletion syndrome [MIM 613675] is a rare disorder caused by the haploinsufficiency of *NF1* and contiguous genes. NF1-microdeleted patients carry a heterozygous deletion of 17q11.2 region typically spanning about 1-1.4 Mb.[1,2] NF1 microdeletion syndrome is often characterized by a more severe phenotype compared to the one observed in NF1 with intragenic mutation.[3] Comparing the clinical phenotype between NF1-microdeleted patients and the whole NF1 population, we found that cardiovascular malformations (CVMs) are significantly more frequent in NF1 patients with microdeletion syndrome than in those with neurofibromatosis caused by intragenic mutation.[4] The CMVs found in the NF1-deleted patients include pulmonic stenosis, atrial/ventricular septal defects and valve defects, and show an incidence of 18% versus 2.1% displayed by NF1 patients with intragenic mutation.[4,5]

The higher incidence of CVMs in NF1-microdeleted patients is most likely dependent on the haploinsufficiency of genes lying in the deletion interval, presumably involved in heart morphogenesis. Our previous search for candidate genes by Northern blotting and RT-PCR analysis evidenced that three genes encompassed by NF1 microdeletion, *SUZ12*, *ADAP2* (formerly *CENTA2*) and *UTP6* (formerly *C17ORF40*) are highly expressed in human fetal heart and during the early developmental stages of mouse embryonic heart,[6] thus deserving further analysis.

SUZ12 (*Suppressor of Zeste 12 Homolog (Drosophila)*) is the human ortholog of the Drosophila *Su(z)12* polycomb gene, encoding a protein which is implicated in developmental mechanisms in Drosophila.[7] Mice lacking *Suz12* are not viable and die around 7.5 days post coitum (dpc), displaying severe developmental and proliferative defects.[8]

ADAP2 (*ArfGAP with Dual PH domains 2*) encodes a protein named Centaurin-alpha-2, which belongs to the centaurins protein family. Centaurin-alpha-2 is recruited to the plasma membrane where it specifically regulates actin cytoskeleton remodeling via ARF6, indicating an important role in exocytosis and cell motility.[9] Moreover, it was recently shown to interact with microtubules and to increase their stability.[10]

UTP6 (*small subunit (SSU) processome component, homolog (yeast)*) is the human homolog of yeast *small subunit (SSU) processome component*. The *UTP6* gene is essential for efficient pre-rRNA processing [11] and seems to be involved in the positive regulation of apoptosis.[12]

Here, we investigated the spatio-temporal expression profile of *ADAP2*, *SUZ12* and *UTP6* murine orthologs during mouse embryonic and fetal development by in situ hybridization. Based on this analysis, we held *ADAP2* the most interesting candidate gene for CVMs occurrence and used zebrafish as a model organism to investigate *in vivo* the role of *adap2*, the *ADAP2* zebrafish ortholog, during vertebrate heart development by loss-of-function experiments.

RESULTS

Expression analysis of *Suz12*, *Utp6* and *Adap2* genes in mouse reveals that *Adap2* is Expressed During Key Stages of Heart Development

In order to elucidate the expression pattern of *Suz12*, *Utp6* and *Adap2* genes in mouse, we performed *in situ* hybridizations using whole mounts at different stages of development, ranging from 7.5 to 11.5 dpc.

The gene which revealed the most interesting expression pattern was *Adap2*, since it was visible in heart between 9 dpc and 10.5 dpc (figure 1) during fundamental phases of cardiac morphogenesis, namely heart looping (beginning at 8 dpc), endocardial cushion formation (10 dpc), and septation of the outflow tract, atria, and ventricles (10.5 dpc). In particular, the strongest *Adap2* mRNA hybridization signal was seen in the heart atria and ventricles at 9.5 dpc (figure 1E), but its expression in the heart was visible as of 9 dpc (figure 1C) and was still present in both atria and ventricles at 10.5 dpc (figure 1F). We also performed *in situ* hybridizations on cryosections of 15.5 dpc embryos in order to assess if *Adap2* transcript is also present in the heart during the later stages of fetal cardiac development. Our experiments demonstrated that the expression of *Adap2* in the heart continues to be maintained at least until 15.5 dpc, in both the ventricles and atria (figure 1H).

Conversely, *Suz12* evidenced a more spatially and temporally restricted expression in heart, with a clear hybridization signal only at 10.5 dpc in the atrium, while *Utp6* revealed no expression in heart at any analyzed stages (figure S1).

Based on this evidence, we held *ADAP2* the most interesting candidate gene for CVMs occurrence and we used zebrafish as a model organism to investigate *in vivo* its role during vertebrate heart development.

adap2, the _ADAP2_ Zebrafish Ortholog, is Required for Proper Cardiac Morphogenesis

In order to explore the spatio-temporal expression pattern of *adap2*, the *ADAP2* zebrafish ortholog (Ensembl Gene ID: ENSDARG00000070565), we performed RT-PCR and whole mount *in situ* hybridization assays. *adap2* transcript was detected by RT-PCR at all analyzed stages, from cleavage up to 120 hpf (hours post fertilization), as well as in the oocytes, indicating that the gene is both maternally and zygotically expressed. Furthermore, *adap2* mRNA was present in all analyzed adult tissues, including heart (figure S2). Whole-mount *in situ* hybridization revealed that *adap2* transcript was present in the heart at 2 dpf (days post fertilization) and 3 dpf stages, in the region corresponding to bulbus arteriosus (figure S2).

In order to investigate the potential role of *adap2* during zebrafish heart development *in vivo*, we performed loss-of-function experiments by injecting two independent translation-blocking morpholinos (*adap2*-MO and UTR-*adap2*-MO) which target the region surrounding *adap2* translation start codon and the 5'-UTR region, respectively. The injection of a control morpholino (std-MO) with no targets in zebrafish was used as control of the microinjection. At 2 dpf, most of embryos injected with 0.3 pmol of *adap2*-MO (morphants), unlike std-MO injected embryos, displayed blood circulation defects and curved tail (figure 2). Lower doses caused no circulatory defects. For the analysis of injected embryos, we focused our attention on 2 dpf, stage at which the circulation is surely started and the cardiac looping occurred in control embryos. At this stage, 61% (n=94) of embryos injected with 0.3 pmol/embryo of *adap2*-MO showed one or more blood

circulatory defects, such as the total loss of circulation (21%), accumulation of blood cells in the trunk and/or tail region (48%) and blood stases in the head (13%) (figure 2D-F,G). All these circulatory defects were noticed in both *adap2* morphants which showed a body axis comparable to that of control embryos and morphants which displayed a bent tail phenotype (71%, n=94). The injection of the second translation-blocking MO, UTR-*adap2*-MO, caused *in vivo* qualitatively similar defects to the first injected MO, though with a different penetrance (figure S3).

To rule out that circulation defects could be caused by alterations of vascular development, we carried out *adap2* loss-of-function experiments in the tg(*flk1*:EGFP) zebrafish transgenic line,[13] where EGFP expression is controlled by the endothelial specific *flk1* promoter (figure S4; figure S5). At 2 dpf, *adap2* knocked down embryos revealed no gross defects in vascular development, with correct development of main axial vessels, Dorsal Aorta (DA) and Cardinal Vein (CV), indicating a normal vasculogenesis. Weak defects in intersomitic vessels (Se) were observed only in those embryos with a marked curved tail, suggesting that these alterations were likely caused by structural defects of body axis rather than by angiogenesis abnormalities.

The evidence that two independent morpholinos gave the same *in vivo* phenotypes confirmed the specificity of the *adap2* morpholinos. Consequently, we present here data obtained on embryos injected with the *adap2*-MO, which we indicate as *adap2* morphants.

The evidence that circulatory defects in *adap2* morphants were not caused by vascular defects suggested that they were most likely derived from an abnormal heart development and functionality. To test this hypothesis, we injected *adap2*-MO or std-MO in embryos belonging to the tg(*gata1*:dsRed)^{sd2};tg(*flk1*:EGFP)^{S843} double transgenic line,[14] in which erythrocytes are labeled in red and endothelial cells are labeled in green; we observed the injected embryos under a confocal microscope (figure 3). At 2 dpf, control embryos displayed a normal heart morphology (figure 3A), while *adap2* morphants showed a reduction of atrioventricular (AV) canal bending, a partial lack of atrium and ventricle separation, as well as a reduced ventricle size (figure 3B-C). All analyzed embryos displayed blood circulation.

The *in vivo* analysis of *adap2* phenotype in morphants prompted us to investigate their heart morphology by a molecular approach, through whole mount *in situ* hybridization assays with the cardiac specific marker *cmlc2* (*cardiac myosin light chain 2*) (figure 4, table S1, table S2). At 26 hpf, std-MO injected embryos showed the linear cardiac tube correctly positioned ventrally in the left region of the embryo (left jog) (figure 4A). On the contrary, only 39% (n=59) of *adap2*-MO injected embryos displayed, at the same stage, the correct leftward cardiac jogging (figure 4B), while another 39% showed no jog, with the heart tube situated centrally along the midline of the embryo (figure 4C). Finally, the remaining 22% of *adap2* morphants was characterized by an inverted cardiac jogging (right jog) (figure 4D). At 2 dpf, std-MO injected embryos hybridized with the *cmlc2* specific probe presented a normal S-shaped heart with the ventricle positioned on the right of the atrium, indicating a correct D-looping process (figure 4E). Differently, only 22% (n=49) of *adap2* morphants showed a heart morphology comparable to control embryos (figure 4F). The remaining *adap2* injected embryos displayed either an intermediate phenotype with reduced looping (18%), or absence of looping with a completely linear heart tube (47%), or a reversed heart looping with the ventricle on the left of the atrium (12%) (figure 4G-I). Moreover, whole mount *in situ* hybridization assays with the ventricle specific marker *vmhc (ventricular myosin heavy chain)* evidenced, at 2 dpf, a marked reduction of ventricle size in 64% (n=39) of *adap2* morphants, confirming the *in vivo* observations (figure S6). The reduction of ventricle size was observed regardless of the heart looping phenotype (D-loop, no loop or reversed loop). Notably, the percentage of embryos showing reduced ventricle size was similar in *adap2* morphants with or without blood circulation, 65% (n=29) and 60% (n=10) respectively, suggesting no relation between this defect and circulatory complications.

adap2 Loss-Of-Function Affects Atrioventricular Valve Development

In order to shed light on the effect of *adap2* knockdown on cardiac functionality, we analyzed AV valve formation in zebrafish by carrying out histological sections of AV valve in std-MO and

adap2-MO injected embryos at different developmental stages. At 3 dpf stage, control embryos displayed correctly formed endocardial cushions in the AV canal connecting the two cardiac chambers (figure 5A). The *adap2* morphants morphologically more similar to std-MO injected embryos still showed proper heart morphology with normal endocardial cushions, the only evident defect being a mild reduction of ventricle size, as already evidenced (figure 5B). In *adap2* injected embryos which *in vivo* showed an intermediate phenotype (bent tail and presence of blood circulation), a visible alteration of the endocardial cushions was observed, with a marked disorganization of the cellular elements that will be forming the mature AV valve (figure 5C). Embryos with severe phenotype, i.e. curved tail and absent circulation, showed serious alterations in the heart morphology, making impossible any consideration on endocardial cushion formation (figure 5D). The histological analysis of std-MO injected embryos at 5 dpf evidenced a properly developed mature valve, recognizable as two flap-like structures in correspondence to the AV canal (figure 5E). At this stage, *adap2*-MO injected embryos showing an *in vivo* mild phenotype were already characterized by evident defects of mature AV valve, whose cells resulted disorganized and poorly compact (figure 5F). The morphology of mature valves in morphants with curved phenotype and with blood circulation appeared more compromised, structurally disorganized, without the typical valvular shape and with cells irregularly disposed (figure 5G). Finally, the most affected *adap2* morphants showed severe cardiac malformations: the heart appeared essentially as a linear-shaped structure, without a clear separation between the two chambers, and consequently it was impossible to analyze mature cardiac valve conformation (figure 5H). Moreover, longitudinal histological sections of *adap2* morphants at 5 dpf evidenced an endocardial detachment from the myocardial layer notably in the atrial chamber (figure 5F-G).

To characterize at molecular level the cardiac AV valve defects displayed by embryos as a consequence of *adap2* functional inactivation we analyzed, by means of *in situ* hybridization experiments, the expression pattern of two markers, *bmp4* (*bone morphogenetic protein 4*) and *notch1b* (*notch homolog 1b*), which at 2 dpf are specifically expressed within the myocardial and

endocardial component of AV canal, respectively (figure 6A,E). At 2 dpf stage, 91% (n=46) of control embryos showed a *bmp4* specific hybridization signal precisely marking the myocardial component of AV canal, as expected (figure 6B). Differently, 51% (n=41) of *adap2*-MO injected embryos displayed a disorganized and ectopically expanded *bmp4* specific expression domain, notably as the ventricular chamber is concerned (figure 6C-D). These defects were observed in all the phenotypic classes of heart development. Similar results were obtained from the analysis of *notch1b* marker at the same stage, with 49% (n=43) of *adap2*-MO injected embryos displaying an expanded and disorganized *notch1b* expression pattern (figure 6G-H). All these data highlight *adap2* function in fundamental processes of zebrafish cardiac morphogenesis, notably heart jogging, heart looping, determination of ventricular size and AV valve formation.

Overall, our findings provide compelling evidence that *ADAP2* is involved in heart development, pointing to it as the most plausible candidate gene for the occurrence of congenital CVMs in NF1 microdeletion syndrome and, more generally, for the occurrence of sporadic and familial congenital CVMs.

DISCUSSION

Microdeletion syndromes are a group of disorders characterized by the deletion of a chromosomal segment spanning multiple disease genes, each potentially contributing to the phenotype independently. Microdeletion syndromes are often characterized by a complex clinical and behavioral phenotype resulting from the imbalance of normal dosage of genes located in that particular chromosomal segment.[15]

NF1 microdeletion syndrome is caused by heterozygous deletions involving the *NF1* gene and, in the most common 1.4 Mb deletion, other 14 genes.[2] A more severe clinical phenotype has often been reported in NF1 patients carrying the microdeletion compared to patients with intragenic *NF1* mutations.[3] By reviewing the phenotype of 92 patients with NF1 microdeletion, we found that CVMs occurred at a significantly higher incidence in this patient population as compared to NF1

patients with intragenic mutations,[4] suggesting that the whole gene deletion segment encompasses important genes involved in heart development. Subsequent expression studies indicated three possible candidate genes for CVMs that warranted further studies: *ADAP2* (formerly known as *CENTA2*), *SUZ12* and *UTP6* (previously called *C17ORF40*).[6]

Here, we analyzed the spatio-temporal expression profile of the above mentioned genes during mouse embryonic and fetal development. Based on this analysis, *Adap2* seems to be expressed in heart starting from 9 dpc, during key phases of cardiac development, that is when the heart tube is elongating and looping, and atrial and ventricular septa, as well as AV valves, are forming.[16] Moreover, *Adap2* expression in heart continues even in the later stages of development, at least until 15.5 dpc. Of note, *Adap2* expression is not restricted to a particular cardiac compartment or structure, but rather seems to localize in both atria and ventricles. *Suz12* was also detected in heart during mouse development, but its expression seems to be restricted to a short period around 10.5 dpc and to the heart atria. Differently, *Utp6* showed no expression in the developing heart at all.

Since the expression of *ADAP2* mouse ortholog in heart during fundamental stages of cardiac morphogenesis was suggestive of a role in heart development, we studied the possible role of *ADAP2* in heart development by employing zebrafish as a model system. Over the recent years, zebrafish has proven to be a valid model for studying cardiovascular development. Despite its apparent simplicity, the zebrafish heart shares common structural, developmental and genetics features with avian and mammalian heart.[17-19] In addition, because of their small size, they receive enough oxygen by passive diffusion from external medium to survive and continue to develop in a relatively normal fashion for several days even in the complete absence of blood circulation, allowing a detailed phenotypic analysis of animals with severe cardiovascular defects that would be lethal in other organisms.[20]

The functional inactivation of *adap2*, the *ADAP2* zebrafish ortholog, obtained by the injection of two MO oligos targeting different *adap2* mRNA regions (translation start site and 5'-UTR), caused the same circulatory defects, proving the specificity of the phenotypes. We also designed a splice-

blocking MO, which was predicted to cause exon 2 skipping and to produce an altered form of *adap2* transcript with the generation of a premature stop codon. However, the injection of this MO at different doses did not cause any evident phenotypic defects. RT-PCR analysis, performed to test the efficacy of the splice-blocking MO, showed that only a fraction of *adap2* mRNA was incorrectly spliced. Consequently, we reason that the partial expression of the wild-type protein could be enough to prevent the occurrence of the phenotypic defects. This evidence, along with the presence in the embryo of the maternal transcript, which is targeted only by translation-blocking MOs, might explain the absence of alterations following the injection of this MO.

Our molecular results suggested *adap2* involvement in the cardiac jogging process, the morphogenetic process in which the heart cone is displaced to the left with respect to the anterior-posterior axis, which is one of the first evident breaks in left-right symmetry of the primitive zebrafish heart tube.[21] Moreover, *adap2* also appeared fundamental for the subsequent D-looping process, the bend of the heart tube to the right, which by 36 hpf leads to the typical S-shaped heart, with the ventricle positioned on the right of the atrium. This was supported by the high number of *adap2* morphants which at 2 dpf, when D-looping is normally completed, showed a linear heart, a reduced loop or a reversed loop, all defects ascribable to alterations of the heart bending taking place during the D-looping process.

Functional inactivation of *adap2* also evidenced its important role during AV valve morphogenesis, since the earliest stages of endocardial cushion formation. Our results strongly suggest that a defective valvulogenesis results in impaired cardiac functionality, therefore AV valve morphological alterations are most likely accounting for the *in vivo* blood circulation defects displayed by *adap2* morphants. Valve defects, including mitral valve prolapse, pulmonary valve stenosis and aortic valve anomalies, constitute a significant proportion of CVMs observed in patients with NF1 microdeletion syndrome.[3,4] Taking into account our findings on *ADAP2* role in valve morphogenesis, a correlation between *ADAP2* haploinsufficiency and the onset of valvular defects in NF1-microdeleted patients can be hypothesized. In addition, the detachment between

endocardium and myocardium observed in *adap2* morphants, particularly in the atrial chamber, could be caused by increased amounts of the extracellular matrix (cardiac jelly) juxtaposed between the two cardiac layers. Normal valve development involves multiple signaling pathways and extracellular matrix components take part in this process. Interestingly, dysregulation of components of the extracellular matrix seems to have a role in the myxomatous degeneration, the leaflet thickening and redundancy, typical of valvular abnormalities, such as mitral valve prolapse.[22]

ADAP2 is known to regulate microtubule stability [10] and the activity of ARF6, a GTPase involved in cellular motility, adhesion and polarity by regulating cytoskeleton remodeling and cortical actin formation [9]. The alteration of these functions might impair adhesion and migration properties of AV valve cells, explaining their disorganization and the irregular valve architecture observed in *adap2* morphants.

During the early phases of valve morphogenesis, the myocardial component of AV junction is fundamental for the signaling events leading endocardial cells to begin the formation of cushions, which will be later remodeled to create flap-like valvular structures.[23] The marked alteration of *bmp4* myocardial expression in *adap2* morphants suggests a compromised signaling from myocardium to endocardium, which might result in the structural valve defects observed at 5 dpf.

Overall, our study points to *ADAP2* as a gene involved in heart development and as a plausible candidate gene for the occurrence of CVMs in NF1-microdeleted patients and in the general population, constituting an advance towards a better comprehension of the complex phenotypic spectrum of the syndrome, as well as of the genetic basis of CVMs.

MATERIALS AND METHODS

Animals

The mice used were of the CD1 strain (Charles River Laboratories International, Inc.) and were housed in the pathogen-free facility at the San Raffaele Scientific Institute (Milano-Italy). Zebrafish (*Danio rerio*) embryos, collected by natural spawning, were raised and maintained according to established techniques.[24] Embryos were staged according to Kimmel and colleagues [25] and raised at 28°C in fish water (Instant Ocean, 0,1% Methylene Blue) in Petri dishes. Beginning from 24 hpf, embryos were cultured in fish water containing 0.003% PTU (1-phenyl-2-thiourea; SIGMA) to prevent pigmentation. The following lines were used: AB (obtained from the Wilson lab, University College London, London, United Kingdom); tg(*flk1*:EGFP) [13] (from the Stainier lab, University of California at San Francisco), tg(*gata1*:dsRed)^{sd2}; tg(*flk1*:EGFP)^{S843} [14] (From the Santoro lab, Molecular Biotechnology Center, Università di Torino, Torino, Italy).

RT-PCR

RT-PCR was performed on total RNA extracted from oocytes, embryos (about 30 embryos per sample) at different developmental stages and adult organs using the TOTALLY RNA isolation kit (Ambion), treated with RQ1 RNase-Free DNase (Promega) and oligo(dT)-reverse transcribed using Super-Script II RT (Invitrogen), according to manufacturers' instructions. The following primers were used for PCR reactions: adap2_fw 5'-GCTTAGACTTCTGGGATG-3', adap2_rev 5'-CGAGATAACGGTTTTCAAGGC-3'. PCR products were loaded and resolved onto 2% agarose gels.

In Situ Hybridization

Probes were isolated by RT-PCR using specific primers (table S3) and cloned into the pCRII-TOPO vector (Invitrogen). Antisense and sense riboprobes were *in vitro* labeled with modified nucleotides (digoxigenin-UTP, Roche). Whole-mount In Situ Hybridization (WISH) was performed on mouse embryos as described in.[26] At least 8 embryos per stage were analyzed. Prehybridization was performed in a formamide-tween20 solution, after which the DIG-labelled riboprobes were added to

the embryos and incubated at 65°. In situ hybridization on mouse cryostat sections was performed according to.[27]

WISH on zebrafish embryos was substantially carried out as described in [28] on embryos fixed for 2 hours at room temperature in 4% paraformaldehyde/phosphate buffered saline, then rinsed with PBS-Tween, dehydrated in 100% methanol and stored at -20°C until processed for WISH.[29] A minimum of 20 embryos/time point were analyzed.

The following probes were synthesized as described in the corresponding papers: *cmlc2* and *vmhc*, [30] *notch1b* [31] and *bmp4*.[32]

Images of stained embryos were taken with a Leica MZFLIII epifluorescence stereomicroscope equipped with a DFC 480 digital camera and IM50 Leica imaging software (Leica).

For histological sections, stained embryos were re-fixed in 4% PFA, dehydrated, wax embedded, sectioned (8 μm) by a microtome (Leitz 1516) and stained with eosin. Images were taken with an Olympus BH2 microscope, equipped with a Leica DFC 320 digital camera and the IM50 software (Leica).

Morpholino Injections and Phenotype Analysis

Antisense morpholinos (MOs; Gene Tools) were designed against the AUG translation start site region and the coding sequence, *adap2*-MO (5'-TTGTTCTTTTCCCGATTTGCCATAG-3') and against the 5'-UTR region, UTR-*adap2*-MO (5'- AAAACACTCCTGTCGCGTCAGAATC-3'). As a control for unspecific effects, each experiment was performed in parallel with a std-MO (standard control oligo) with no target in zebrafish.

All morpholinos were diluted in Danieau solution [33] and injected at 1-2 cells stage. Rhodamine dextran (Molecular Probes) was usually co-injected as a tracer. After injection, embryos were raised in fish water at 28ºC and observed up to the stage of interest. For a better observation, the injected embryos were anaesthetized using 0.016% tricaine (Ethyl 3-aminobenzoate methanesulfonate salt, SIGMA) in fish water.

Images were acquired by using a Leica MZ FLIII epifluorescence microscope equipped with a Leica DCF 480 digital camera and the IM50 software (Leica). Confocal microscopy was performed with a Leica TCSNT confocal microscope equipped with an Ar/Kr laser (blocking filter BP 530/30 for EGFP and blocking filter LP 590 for ds Red).

For histological analysis 3 dpf and 5 dpf zebrafish early larvae were fixed overnight at 4°C with bouin fixative. The samples were then dehydrated in a graded ethanol series, wax embedded, sectioned (8 μm) by a microtome (Leitz 1516) and stained with hematoxylin/eosin. Images were taken with a Leica DM6000 B microscope equipped with a Leica DCF480 digital camera and the LAS software.

ACKNOWLEDGMENTS

We thank U. Fascio for his help in the acquisition of confocal images.

COMPETING INTERESTS

None.

FUNDING

This work was supported by PUR, Italy to PR.

REFERENCES

1. Venturin M, Gervasini C, Orzan F, Bentivegna A, Corrado L, Colapietro P, Friso A, Tenconi R, Upadhyaya M, Larizza L, Riva P. Evidence for nonhomologous end joining and non allelic homologous recombination in atypical NF1 microdeletions. *Hum Genet* 2004;**115**:69-80

2. Pasmant E, Sabbagh A, Spurlock G, Laurendeau I, Grillo E, Hamel MJ, Martin L, Barbarot S, Leheup B, Rodriguez D, Lacombe D, Dollfus H, Pasquier L, Isidor B, Ferkal S, Soulier J, Sanson M, Dieux-Coeslier A, Bièche I, Parfait B, Vidaud M, Wolkenstein P, Upadhyaya M, Vidaud D. NF1 microdeletions in neurofibromatosis type 1: from genotype to phenotype. *Hum Mutat* 2010;**31**:E1506-18

3. Mautner VF, Kluwe L, Friedrich RE, Roehl AC, Bammert S, Högel J, Spöri H, Cooper DN, Kehrer-Sawatzki H. Clinical characterisation of 29 neurofibromatosis type-1 patients with molecularly ascertained 1.4 Mb type-1 NF1 deletions. *J Med Genet* 2010;**47**:623-30

4. Venturin M, Guarnieri P, Natacci F, Stabile M, Tenconi R, Clementi M, Hernandez C, Thompson P, Upadhyaya M, Larizza L, Riva P. Mental retardation and cardiovascular malformations in NF1 microdeleted patients point to candidate genes in 17q11.2. *J Med Genet* 2004;**41**:35-41

5. Lin AE, Birch PH, Korf BR, Tenconi R, Niimura M, Poyhonen M, Armfield Uhas K, Sigorini M, Virdis R, Romano C, Bonioli E, Wolkenstein P, Pivnick EK, Lawrence M, Friedman JM. Cardiovascular malformations and other cardiovascular abnormalities in neurofibromatosis 1. *Am J Med Genet* 2000;**95**:108-17

6. Venturin M, Bentivegna A, Moroni R, Larizza L, Riva P. Evidence by expression analysis of candidate genes for congenital heart defects in the NF1 microdeletion interval. *Ann Hum Genet* 2005;**69**:508-16

7. Kuzmichev A, Nishioka K, Erdjument-Bromage H, Tempst P, Reinberg D. Histone methyltransferase activity associated with a human multiprotein complex containing the Enhancer of Zeste protein. *Genes Dev* 2002;**16**:2893-2905

8. Pasini D, Bracken AP, Jensen MR, Lazzerini Denchi E, Helin K. Suz12 is essential for mouse development and for EZH2 histone methyltransferase activity. *EMBO J* 2004;**23**:4061-4071

9. Venkateswarlu K, Brandom KG, Yun H. PI-3-kinase-dependent membrane recruitment of centaurin-alpha2 is essential for its effect on ARF6-mediated actin cytoskeleton reorganisation. *J Cell Sci* 2007;**120**:792-801

10. Zuccotti P, Cartelli D, Stroppi M, Pandini V, Venturin M, Aliverti A, Battaglioli E, Cappelletti G, Riva P. Centaurin-a2 Interacts with b-Tubulin and Stabilizes Microtubules. *PLoS ONE* 2012;**7**: e52867

11. Champion EA, Lane BH, Jackrel ME, Regan L, Baserga SJ. A direct interaction between the Utp6 half-a-tetratricopeptide repeat domain and a specific peptide in Utp21 is essential for efficient pre-rRNA processing. *Mol Cell Biol* 2008;**28**:6547-56

12. Piddubnyak V, Rigou P, Michel L, Rain JC, Geneste O, Wolkenstein P, Vidaud D, Hickman JA, Mauviel A, Poyet JL. Positive regulation of apoptosis by HCA66, a new Apaf-1 interacting protein,

and its putative role in the physiopathology of NF1 microdeletion syndrome patients. *Cell Death Differ* 2007;**14**:1222-33

13. Jin SW, Beis D, Mitchell T, Chen JN, Stainier DY. Cellular and molecular analyses of vascular tube and lumen formation in zebrafish. *Development* 2005;**132**:5199-5209

14. Santoro MM, Samuel T, Mitchell T, Reed JC, Stainier DY. Birc2 (clap1) regulates endothelial cell integrity and blood vessel homeostasis. *Nat Genet* 2007;**39**:1397-1402

15. Shaffer LG, Ledbetter DH, Lupski JR. Molecular cytogenetics of contiguous gene syndromes: Mechanisms and consequences. In: Scriver CR, Beaudet AL, Sly WS, Valle D, Childs B, Kinzler KW, Vogelstein B, eds. The metabolic and molecular bases of inherited diseases. New York: McGraw-Hill 2001:6077-96

16. Savolainen SM, Foley JF, Elmore SA. Histology atlas of the developing mouse heart with emphasis on E11.5 to E18.5. *Toxicol Pathol* 2009;**37**:395-414

17. Weinstein BM, Fishman MC. Cardiovascular morphogenesis in zebrafish. *Cardiovas Res* 1996;**31**:E17-24

18. Stainier DY, Fouquet B, Chen JN, Warren KS, Weinstein BM, Meiler SE, Mohideen MA, Neuhauss SC, Solnica-Krezel L, Schier AF, Zwartkruis F, Stemple DL, Malicki J, Driever W, Fishman MC. Mutations affecting the formation and function of the cardiovascular system in the zebrafish embryo. *Development* 1996;**123**:285-92

19. Fishman MC, Stainier DY, Breitbart RE, Westerfield M. Zebrafish: Genetic and embryological methods in a transparent vertebrate embryo. *Meth Cell Biol* 1997;**52**:67-82

20. Stainier DY, Fishman MC. Patterning the zebrafish heart tube: acquisition of anteroposterior polarity. *Dev Biol* 1992;**153**:91-101

21. Chen JN, van Eeden FJ, Warren KS, Chin A, Nüsslein-Volhard C, Haffter P, Fishman MC. Left-right pattern of cardiac BMP4 may drive asymmetry of the heart in zebrafish. *Development* 1997;**124**:4373-82

22. Hayek E, Gring GN, Griffin BP. Mitral valve prolapse. *Lancet* 2005;**365**:507-18

23. Stainier DY. Zebrafish genetics and vertebrate heart formation. *Nat Rev Genet* 2001;**2**:39-48

24. Westerfield M. The Zebrafish Book. Eugene, OR: University of Oregon Press 1993

25. Kimmel CB, Ballard WW, Kimmel SR, Ullmann B, Schilling TF. Stages of embryonic development of the zebrafish. *Dev Dyn* 1995;**203**:253-310

26. Avilion AA, Bell DM, Lovell-Badge R. Micro-capillary tube in situ hybridisation: a novel method for processing small individual samples. *Genesis* 2000;**27**:76-80

27. Strähle U, Blader P, Adam J, Ingham PW. A simple and efficient procedure for non-isotopic in situ hybridization to sectioned material. *Trends Genet* 1994;**10**:75-6

28. Thisse C, Thisse B, Schilling TF, Postlethwait JH. Structure of the zebrafish snail1 gene and its expression in wild-type, spadetail and no tail mutant embryos. *Development* 1993;**119**:1203-15

29. Jowett T, Lettice L. Whole-mount in situ hybridizations on zebrafish embryos using a mixture of digoxigenin- and fluorescein-labelled probes. *Trends Genet* 1994;**10**:73-4

30. Yelon D, Horne SA, Stainier DY. Restricted expression of cardiac myosin genes reveals regulated aspects of heart tube assembly in zebrafish. *Dev Biol* 1999;**214**:23-37

31. Westin J, Lardelli M. Three novel *Notch* genes in zebrafish: implications for vertebrate *Notch* gene evolution and function. *Dev Genes Evol* 1997;**207**:51-63

32. Nikaido M, Tada M, Saji T, Ueno N. Conservation of BMP signaling in zebrafish mesoderm patterning. *Mech Dev* 1997;**61**:75-88

33. Nasevicius A, Ekker SC. Effective targeted gene 'knockdown' in zebrafish. *Nat Genet* 2000;**26**:216-20

LEGENDS TO FIGURES

Figure 1

Expression of *Adap2* in Whole Mount Mouse Embryos and Mouse Cryosections. (A-G) Whole mount *in situ* hybridization on embryos from 8.25 dpc to 11.5 dpc with an *Adap2* specific probe. (A) 8.25 dpc, expression at the midbrain/hindbrain boundary. (B) 8.5 dpc, expression in the gut tube. (C) 9 dpc, expression in forebrain, midbrain, hindbrain, heart (arrow), otic vesicles, gut tube. (D) 9.25 dpc, expression in forebrain, midbrain, hindbrain, otic vesicles, heart (arrow), posterior part of the gut tube. (E) 9.5 dpc, expression in forebrain, midbrain, hindbrain, otic vesicles, heart (arrow), gut tube. (F) 10.5 dpc, expression in forebrain, midbrain, hindbrain, otic vesicles, heart (arrow), gut tube. (G) 11.5 dpc expression in midbrain, inner ear, forelimbs, weakly in hindlimbs. (H) *In situ* hybridization on cryosection of a 15.5 dpc embryo showing *Adap2* expression in heart atrium (a) and ventricle (v).

Figure 2

***adap2* Knockdown Causes Circulation Defects in Zebrafish.** (A) Lateral view and (B) detailed image of the trunk-tail region of std-MO injected embryos at 2 dpf. (C, E-F) Lateral view and (D) detailed image of the trunk-tail region of *adap2*-MO injected embryos at 2 dpf. Anterior to the left. Black arrows: blood stases in the tail region; arrowhead: blood stasis in the head. (G) Percentage of circulation defects in *adap2* morphants at 2 dpf (n=94): 21% of the *adap2* morphants displayed no blood circulation, 48% blood stases in the trunk-tail region and 13% blood stases in the cephalic region.

Figure 3

***adap2* Loss-of-Function Affects Normal Heart Morphogenesis in Zebrafish.** The hearts of double transgenic tg(*gata1*:dsRed)^{sd2};tg(*flk1*:EGFP)^{S843} embryos injected with std-MO or *adap2*-

MO were examined *in vivo* by confocal microscopy at 2 dpf. Erythrocytes and endocardium are labeled in red and green, respectively. Confocal images of the heart in (A) std-MO injected embryo, in (B) *adap2* morphant displaying normal morphology and in (C) *adap2*-MO injected embryo with bent tail. All analyzed embryos presented blood circulation.

Figure 4

***adap2* Loss-of-Function Experiments Perturbs Zebrafish Heart Jogging and Heart Looping.** Analysis of *cmlc2* expression by *in situ* hybridization was performed on std-MO and *adap2*-MO injected embryos at 26 hpf and 2 dpf. The heart position in injected embryos was scored as left jog (normal; A-B), no jog (C) and right (reversed) jog (D) at 26hpf and as D-loop (normal; E-F), reduced loop (G), no loop (H) and reversed loop (I) at 2dpf. V: ventricle; A: atrium. (A-D) Dorsal views through the head, anterior to the bottom; (E-I) frontal views, head to the top.

Figure 5

***adap2* Knockdown Impairs the Normal Endocardial Cushions and Mature Valve Formation.** Histological sections of std-MO and *adap2*-MO injected embryos at 3 dpf (transversal sections) and 5 dpf (longitudinal sections) stained with hematoxylin and eosin**.** (A, E) Heart sections of control embryos at 3 dpf (A) and 5 dpf, with magnification of the valve region (E). (B, F) Heart sections of *adap2* morphants with blood circulation and morphology comparable to controls at 3 dpf (B) and 5 dpf, with magnification of the valve region (F). (C, G) Heart sections of *adap2* morphants with blood circulation and bent tail at 3 dpf (C) and 5 dpf, with magnification of the valve region (G). (D, H) Heart sections of *adap2* morphants with no blood circulation and curved tail at 3 dpf (D) and 5 dpf, with magnification of the valve region (H). Arrowheads: endocardial cushions; double arrows: extracellular matrix (cardiac jelly) located between myocardium and endocardium.

Figure 6

The Expression of Atrio-ventricular Boundary Markers is Affected in *adap2* Morphants. analysis of *bmp4* and *notch1b* expression by *in situ* hybridization was performed on std-MO and *adap2*-MO injected embryos at 2 dpf. (A, E) Schematic representation of *bmp4* and *notch1b* expression domain in zebrafish heart at 2 dpf. The myocardium and endocardium specific territories of *bmp4* and *notch1b* expression are depicted in magenta. (B, F) Embryos injected with std-MO displaying a normal hybridization signal. (C-D, G-H) Embryos injected with *adap2*-MO displaying expanded and disorganized *bmp4* and *notch1b* expression domains. Frontal views are shown.

Figure S1

Expression of *Suz12* and *Utp6* in Whole Mount Mouse Embryos. (A-D) Whole mount *in situ* hybridization on embryos from 8.75 dpc to 11.5 dpc with a *Suz12* specific probe. (A) 8.75 dpc, expression in the telencephalic vesicle. (B) 9.5 dpc, expression in the branchial arches, weak signal in the heart (arrow). (C) 10.5 dpc, expression in branchial arches, limb buds, heart atrium (arrow). (D) 11.5 dpc, expression in forebrain, hindbrain, fore and hindlimbs. (E-H) Whole mount *in situ* hybridization on embryos from 9.25 dpc to 11.5 dpc with an *Utp6* specific probe. (E) 9.25 dpc, expression in the branchial arches, weak expression in the forebrain. No hybridization signal in the heart (arrow). (F) 10.25 dpc, expression in branchial arches, limb buds, otic vesicles. (G) 10.75 dpc, expression in branchial arches, limb buds, otic vesicles. (H) 11.5 dpc, expression in forebrain, limb buds, otic vesicles, inner ear.

Figure S2

Spatio-temporal Expression Pattern of *adap2* in Zebrafish. (A) RT-PCR analysis of *adap2* expression in zebrafish, performed on total RNAs extracted from oocytes and different embryonic and larval stages (from 8 cells to 120 hpf) and adult organs. (B-D) *adap2* spatial expression analyzed by WISH at 2 dpf and 3 dpf stages. (B) Lateral views of the cephalic region of 2 dpf and (C) 3 dpf stained embryos oriented with anterior to the left and posterior to the right. (D)

Hystological transverse section of a 2 dpf stained embryo. (B, D) At 2 dpf, *adap2* expression is mainly localized in the cephalic region, with a faint signal in the cardiac region corresponding to the bulbus arteriosus (arrowhead). (C) At 3 dpf, the signal in the cephalic region, as well in the bulbus arteriosus (arrowhead), becomes stronger.

Figure S3

UTR-*adap2*-MO injection gives qualitatively similar results to *adap2*-MO injection, such as circulation defects and blood stases in the trunk/tail and in the head at 2dpf. (A) Lateral view and (B) detailed image of the tail region of std-MO injected embryos. (C, E) Lateral views and (D-F) detailed images of the head and tail region of two different UTR-*adap2*-MO injected embryos. Anterior to the left.Arrowhead: blood stasis in the head; black arrows: blood stases in the tail region. (G) Percentage of circulation defects in UTR-*adap2* morphants at 2 dpf (n=128), after the injection of 0.65 pmol/embryo: 42% of the UTR-*adap2* morphants displayed no blood circulation, 21% blood stases in the trunk-tail region and 5% blood stases in the cephalic region.

Figure S4

***adap2*-MO Injection does not Grossly Affect Vasculogenesis and Angiogenesis at 2 dpf.** *In vivo* analysis of tg(*flk1*:EGFP) embryos injected with (A-D) std-MO or (E-L) *adap2*-MO. (A-B) Bright field images of std-MO injected embryos. (E-F, I) Bright field images of *adap2*-MO injected embryos. (C-D) Fluorescence images of std-MO injected embryos. (G-H, L) Fluorescence images of *adap2*-MO injected embryos. (B, D, F, H) Detailed view of the caudal region. Lateral views, anterior to the left. Se: intersomitic vessels; DA: dorsal aorta; CV: caudal vein.

Figure S5

UTR-*adap2*-MO Injection does not Grossly Affect Vasculogenesis and Angiogenesis at 2 dpf similarly to *adap2*-MO Injection. *In vivo* analysis of tg(*flk1*:EGFP) embryos injected with (A-D)

std-MO or (E-L) UTR-*adap2*-MO. (A-B) Bright field images of std-MO injected embryos. (E-F, I-J) Bright field images of UTR-*adap2*-MO injected embryos. (C-D) Fluorescence images of std-MO injected embryos. (G-H, K-L) Fluorescence images of UTR-*adap2*-MO injected embryos. (B, D, F, H, J, L) Detailed views of the caudal region. Lateral views, anterior to the left. Se: intersomitic vessels; DA: dorsal aorta; CV: caudal vein.

Figure S6

Reduction of Ventricle Size in *adap2* Morphants. *In situ* hybridization analysis of *vmhc* performed on std-MO and *adap2*-MO injected embryos at 2 dpf. (A) Embryos injected with std-MO. (B-D) Embryos injected with *adap2*-MO showing a reduced ventricle size. V: ventricle. All embryos are shown in frontal view.

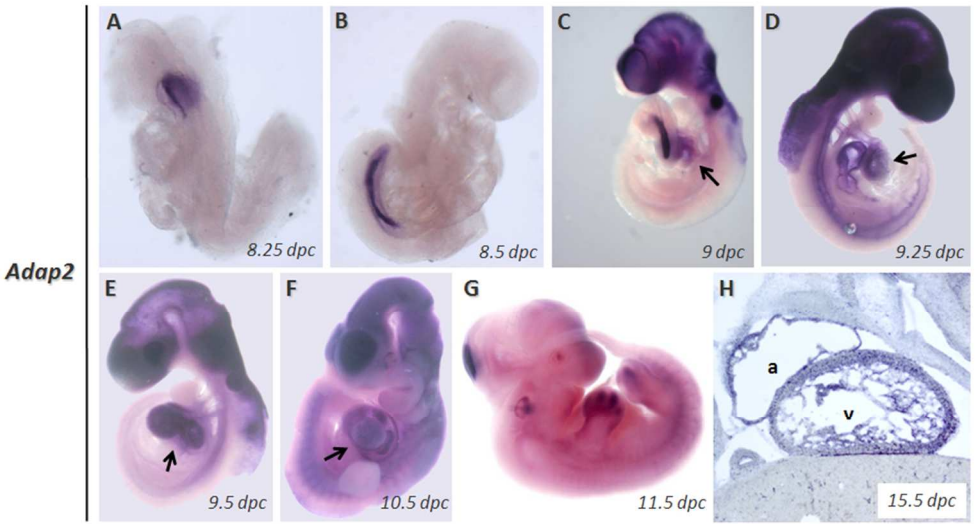

Figure 1
Expression of Adap2 in Whole Mount Mouse Embryos and Mouse Cryosections. (A-G) Whole mount in situ hybridization on embryos from 8.25 dpc to 11.5 dpc with an Adap2 specific probe. (A) 8.25 dpc, expression at the midbrain/hindbrain boundary. (B) 8.5 dpc, expression in the gut tube. (C) 9 dpc, expression in forebrain, midbrain, hindbrain, heart (arrow), otic vesicles, gut tube. (D) 9.25 dpc, expression in forebrain, midbrain, hindbrain, otic vesicles, heart (arrow), posterior part of the gut tube. (E) 9.5 dpc, expression in forebrain, midbrain, hindbrain, otic vesicles, heart (arrow), gut tube. (F) 10.5 dpc, expression in forebrain, midbrain, hindbrain, otic vesicles, heart (arrow), gut tube. (G) 11.5 dpc expression in midbrain, inner ear, forelimbs, weakly in hindlimbs. (H) In situ hybridization on cryosection of a 15.5 dpc embryo showing Adap2 expression in heart atrium (a) and ventricle (v).

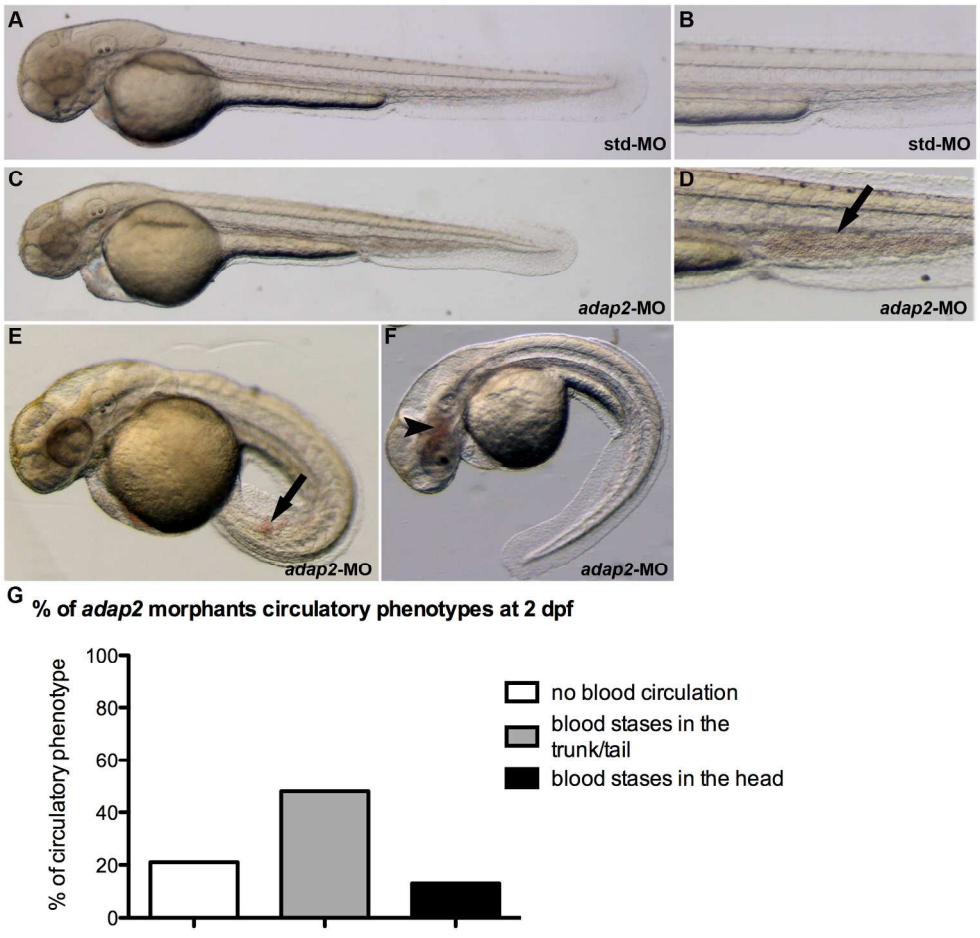

Figure 2
adap2 Knockdown Causes Circulation Defects in Zebrafish. (A) Lateral view and (B) detailed image of the trunk-tail region of std-MO injected embryos at 2 dpf. (C, E-F) Lateral view and (D) detailed image of the trunk-tail region of adap2-MO injected embryos at 2 dpf. Anterior to the left. Black arrows: blood stases in the tail region; arrowhead: blood stasis in the head. (G) Percentage of circulation defects in adap2 morphants at 2 dpf (n=94): 21% of the adap2 morphants displayed no blood circulation, 48% blood stases in the trunk-tail region and 13% blood stases in the cephalic region.

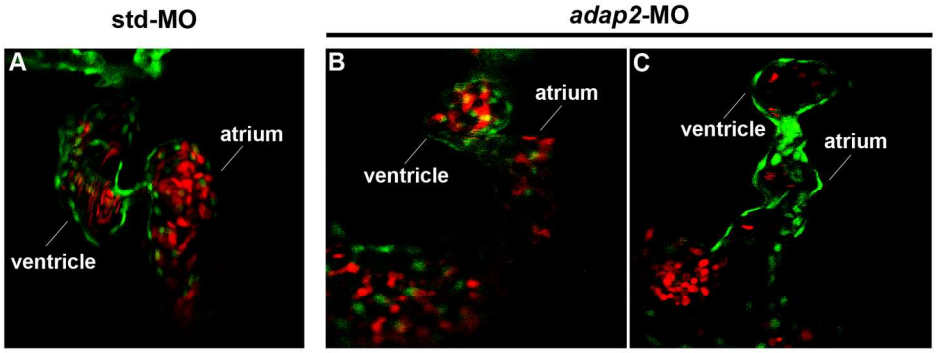

Figure 3
adap2 Loss-of-Function Affects Normal Heart Morphogenesis in Zebrafish. The hearts of double transgenic tg(gata1:dsRed)sd2;tg(flk1:EGFP)S843 embryos injected with std-MO or adap2-MO were examined in vivo by confocal microscopy at 2 dpf. Erythrocytes and endocardium are labeled in red and green, respectively. Confocal images of the heart in (A) std-MO injected embryo, in (B) adap2 morphant displaying normal morphology and in (C) adap2-MO injected embryo with bent tail. All analyzed embryos presented blood circulation.

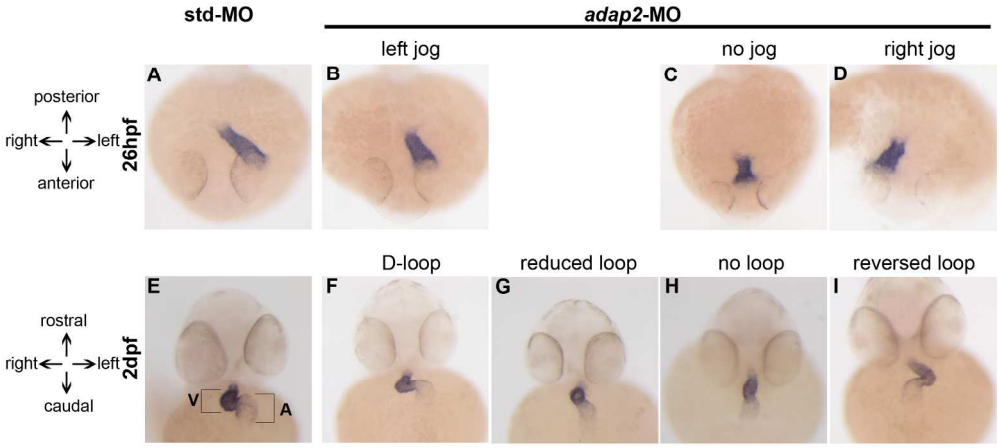

Figure 4
adap2 Loss-of-Function Experiments Perturbs Zebrafish Heart Jogging and Heart Looping. Analysis of cmlc2 expression by in situ hybridization was performed on std-MO and adap2-MO injected embryos at 26 hpf and 2 dpf. The heart position in injected embryos was scored as left jog (normal; A-B), no jog (C) and right (reversed) jog (D) at 26hpf and as D-loop (normal; E-F), reduced loop (G), no loop (H) and reversed loop (I) at 2dpf. V: ventricle; A: atrium. (A-D) Dorsal views through the head, anterior to the bottom; (E-I) frontal views, head to the top.

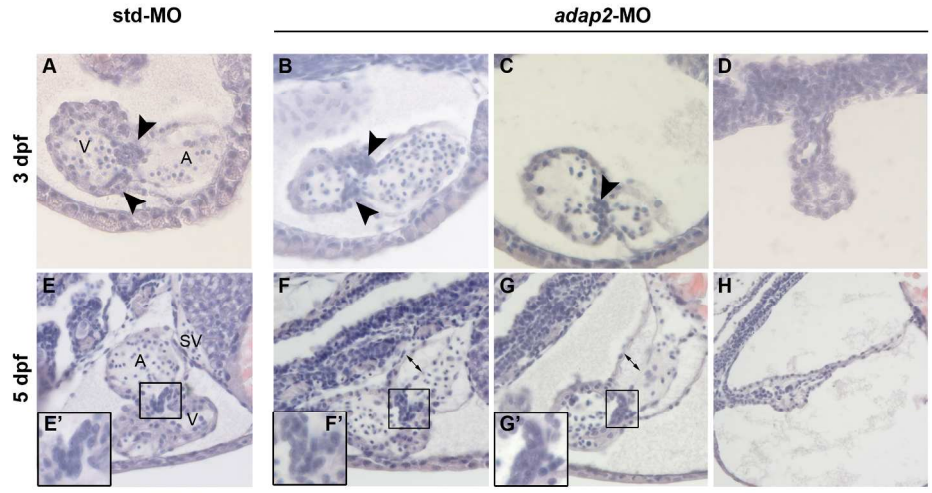

Figure 5
adap2 Knockdown Impairs the Normal Endocardial Cushions and Mature Valve Formation. Histological sections of std-MO and adap2-MO injected embryos at 3 dpf (transversal sections) and 5 dpf (longitudinal sections) stained with hematoxylin and eosin. (A, E) Heart sections of control embryos at 3 dpf (A) and 5 dpf, with magnification of the valve region (E). (B, F) Heart sections of adap2 morphants with blood circulation and morphology comparable to controls at 3 dpf (B) and 5 dpf, with magnification of the valve region (F). (C, G) Heart sections of adap2 morphants with blood circulation and bent tail at 3 dpf (C) and 5 dpf, with magnification of the valve region (G). (D, H) Heart sections of adap2 morphants with no blood circulation and curved tail at 3 dpf (D) and 5 dpf, with magnification of the valve region (H). Arrowheads: endocardial cushions; double arrows: extracellular matrix (cardiac jelly) located between myocardium and endocardium.

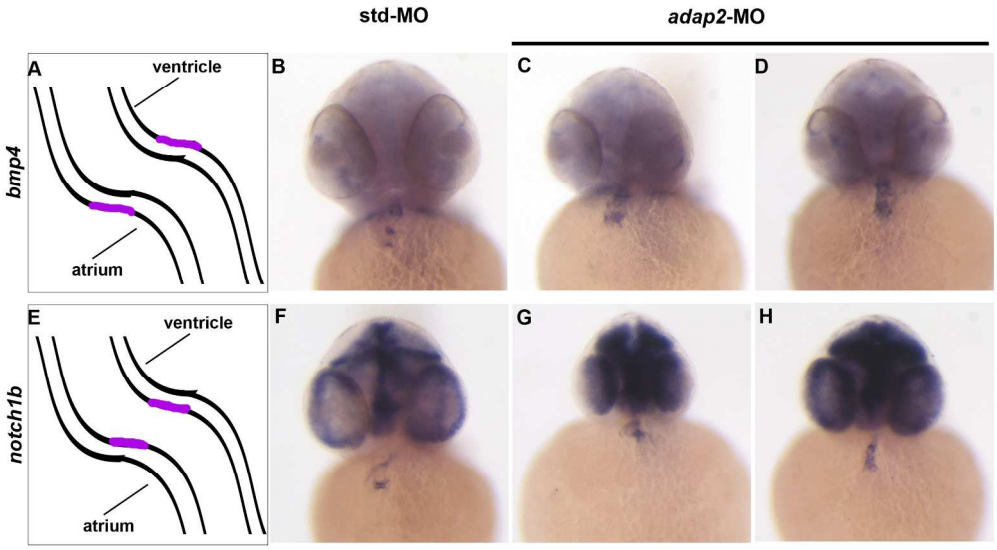

Figure 6
The Expression of Atrio-ventricular Boundary Markers is Affected in adap2 Morphants. analysis of bmp4 and notch1b expression by in situ hybridization was performed on std-MO and adap2-MO injected embryos at 2 dpf. (A, E) Schematic representation of bmp4 and notch1b expression domain in zebrafish heart at 2 dpf. The myocardium and endocardium specific territories of bmp4 and notch1b expression are depicted in magenta. (B, F) Embryos injected with std-MO displaying a normal hybridization signal. (C-D, G-H) Embryos injected with adap2-MO displaying expanded and disorganized bmp4 and notch1b expression domains. Frontal views are shown.

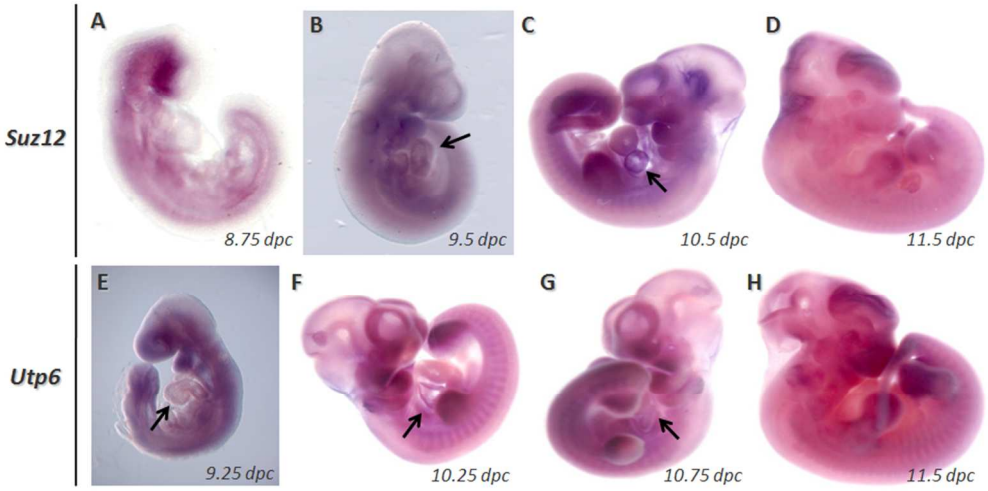

Figure S1
Expression of Suz12 and Utp6 in Whole Mount Mouse Embryos. (A-D) Whole mount in situ hybridization on embryos from 8.75 dpc to 11.5 dpc with a Suz12 specific probe. (A) 8.75 dpc, expression in the telencephalic vesicle. (B) 9.5 dpc, expression in the branchial arches, weak signal in the heart (arrow). (C) 10.5 dpc, expression in branchial arches, limb buds, heart atrium (arrow). (D) 11.5 dpc, expression in forebrain, hindbrain, fore and hindlimbs. (E-H) Whole mount in situ hybridization on embryos from 9.25 dpc to 11.5 dpc with an Utp6 specific probe. (E) 9.25 dpc, expression in the branchial arches, weak expression in the forebrain. No hybridization signal in the heart (arrow). (F) 10.25 dpc, expression in branchial arches, limb buds, otic vesicles. (G) 10.75 dpc, expression in branchial arches, limb buds, otic vesicles. (H) 11.5 dpc, expression in forebrain, limb buds, otic vesicles, inner ear.

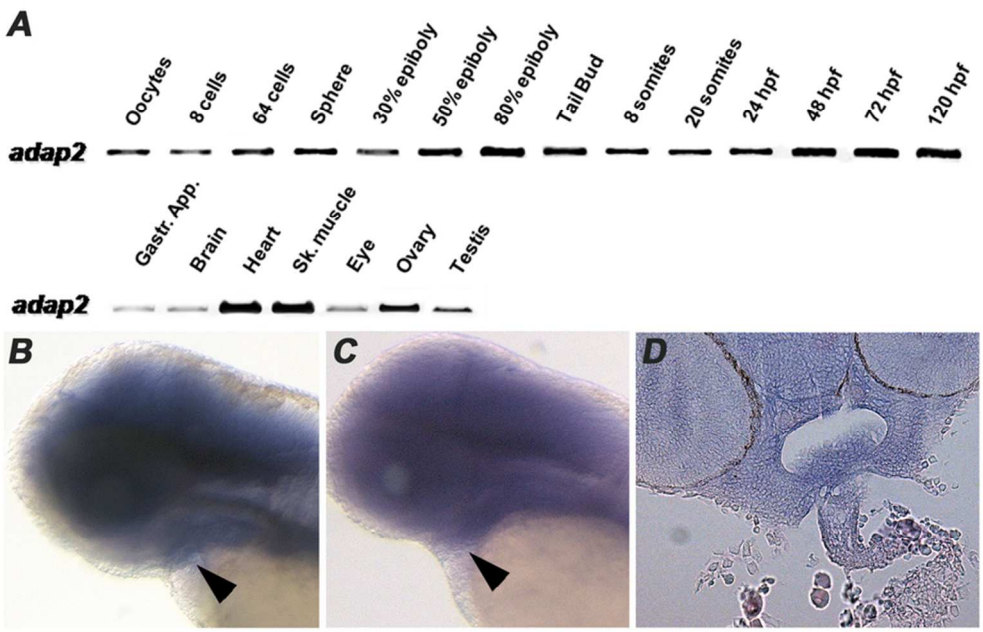

Figure S2
Spatio-temporal Expression Pattern of adap2 in Zebrafish. (A) RT-PCR analysis of adap2 expression in zebrafish, performed on total RNAs extracted from oocytes and different embryonic and larval stages (from 8 cells to 120 hpf) and adult organs. (B-D) adap2 spatial expression analyzed by WISH at 2 dpf and 3 dpf stages. (B) Lateral views of the cephalic region of 2 dpf and (C) 3 dpf stained embryos oriented with anterior to the left and posterior to the right. (D) Hystological transverse section of a 2 dpf stained embryo. (B, D) At 2 dpf, adap2 expression is mainly localized in the cephalic region, with a faint signal in the cardiac region corresponding to the bulbus arteriosus (arrowhead). (C) At 3 dpf, the signal in the cephalic region, as well in the bulbus arteriosus (arrowhead), becomes stronger.
79x51mm (300 x 300 DPI)

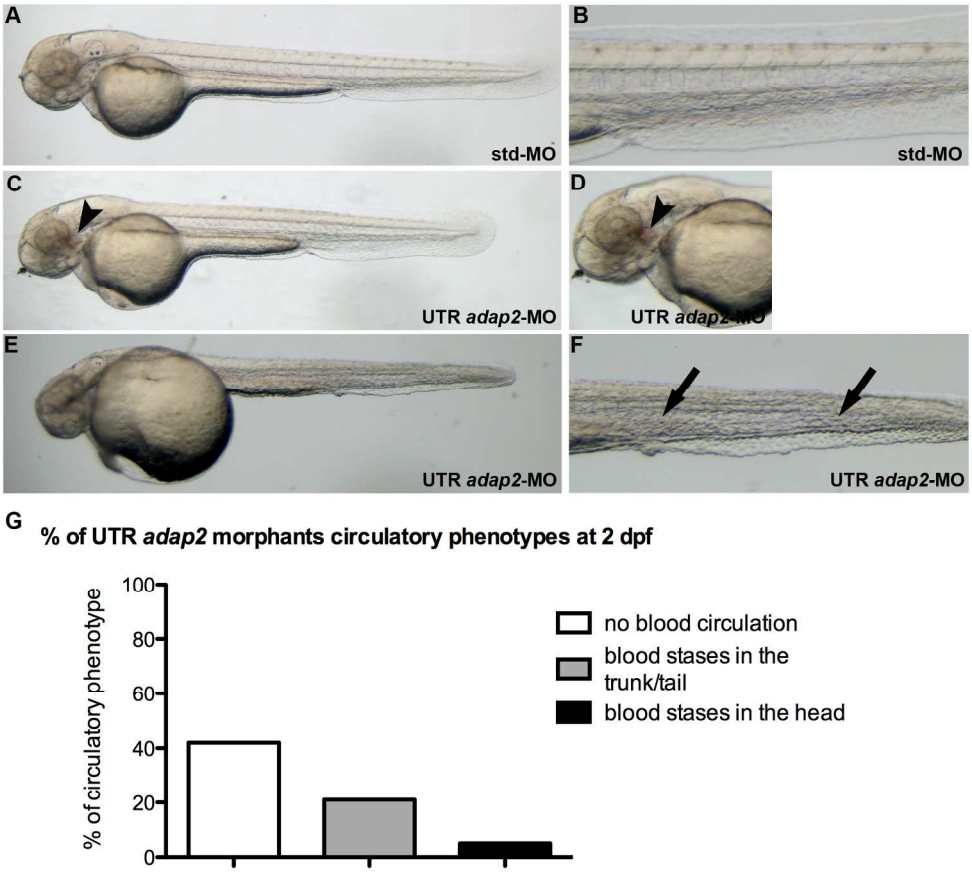

Figure S3

UTR-adap2-MO injection gives qualitatively similar results to adap2-MO injection, such as circulation defects and blood stases in the trunk/tail and in the head at 2dpf. (A) Lateral view and (B) detailed image of the tail region of std-MO injected embryos. (C, E) Lateral views and (D-F) detailed images of the head and tail region of two different UTR-adap2-MO injected embryos. Anterior to the left.Arrowhead: blood stasis in the head; black arrows: blood stases in the tail region. (G) Percentage of circulation defects in UTR-adap2 morphants at 2 dpf (n=128), after the injection of 0.65 pmol/embryo: 42% of the UTR-adap2 morphants displayed no blood circulation, 21% blood stases in the trunk-tail region and 5% blood stases in the cephalic region.

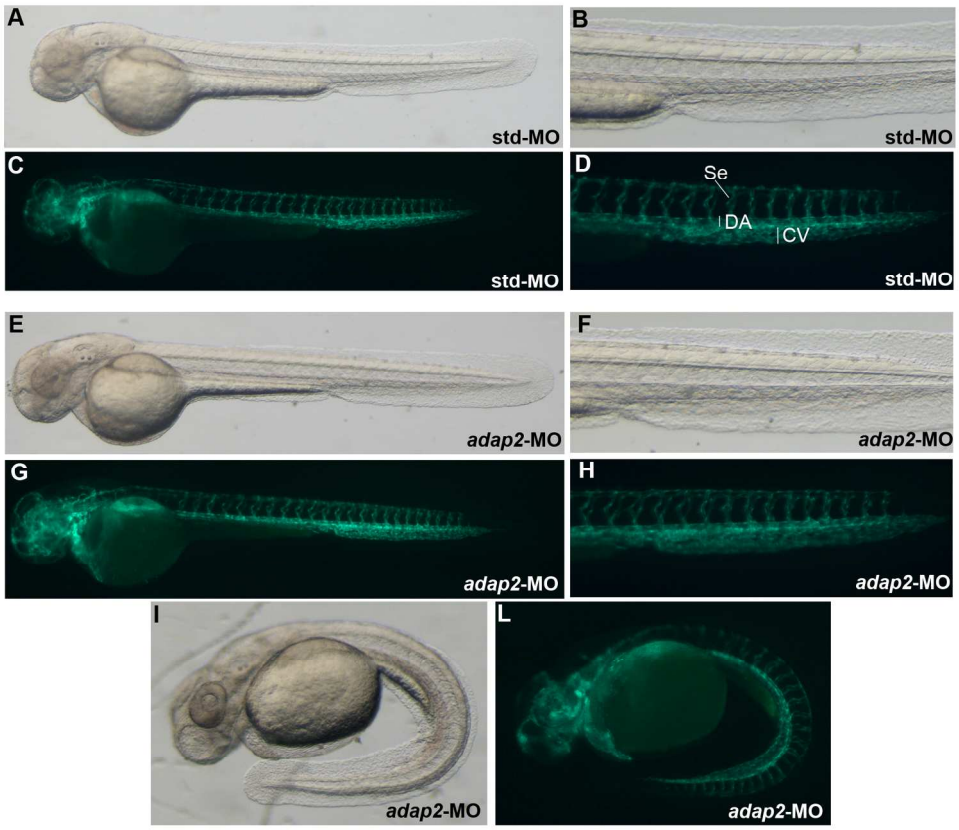

Figure S4
adap2-MO Injection does not Grossly Affect Vasculogenesis and Angiogenesis at 2 dpf. In vivo analysis of tg(flk1:EGFP) embryos injected with (A-D) std-MO or (E-L) adap2-MO. (A-B) Bright field images of std-MO injected embryos. (E-F, I) Bright field images of adap2-MO injected embryos. (C-D) Fluorescence images of std-MO injected embryos. (G-H, L) Fluorescence images of adap2-MO injected embryos. (B, D, F, H) Detailed view of the caudal region. Lateral views, anterior to the left. Se: intersomitic vessels; DA: dorsal aorta; CV: caudal vein.

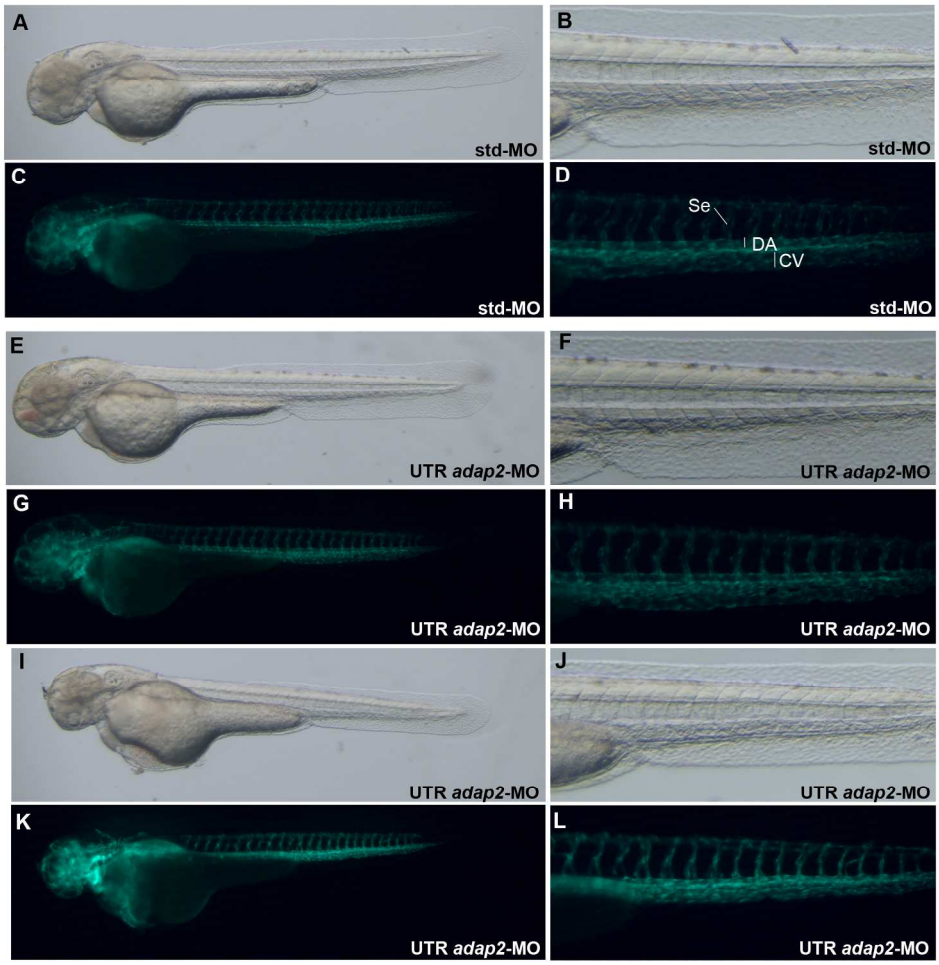

Figure S5
UTR-adap2-MO Injection does not Grossly Affect Vasculogenesis and Angiogenesis at 2 dpf similarly to adap2-MO Injection. In vivo analysis of tg(flk1:EGFP) embryos injected with (A-D) std-MO or (E-L) UTR-adap2-MO. (A-B) Bright field images of std-MO injected embryos. (E-F, I-J) Bright field images of UTR-adap2-MO injected embryos. (C-D) Fluorescence images of std-MO injected embryos. (G-H, K-L) Fluorescence images of UTR-adap2-MO injected embryos. (B, D, F, H, J, L) Detailed views of the caudal region. Lateral views, anterior to the left. Se: intersomitic vessels; DA: dorsal aorta; CV: caudal vein.

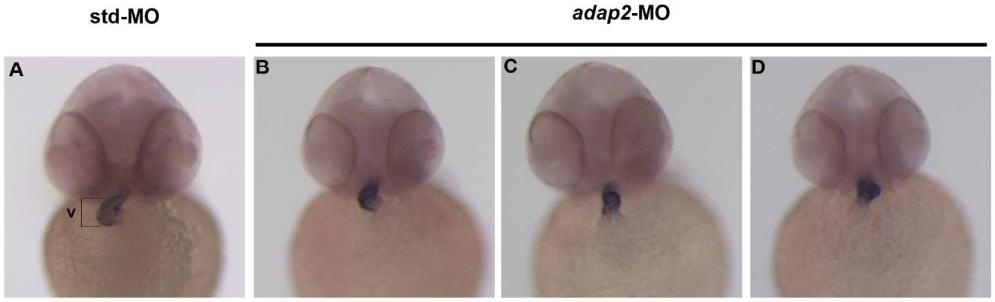

Figure S6
Reduction of Ventricle Size in adap2 Morphants. In situ hybridization analysis of vmhc performed on std-MO and adap2-MO injected embryos at 2 dpf. (A) Embryos injected with std-MO. (B-D) Embryos injected with adap2-MO showing a reduced ventricle size. V: ventricle. All embryos are shown in frontal view.

TABLES

Table S1: heart jogging defects in std-MO and *adap2*-MO injected embryos at 26 hpf as shown by *cmlc2* expression pattern analysis (Figure 4). n. = total number of injected embryos.

		Heart jog (%)			
Injected morpholino	**n.**	Left jog	No jog	Right jog	Total heart jogging defects
std-MO	53	98	2	0	2
adap2-MO	59	39	39	22	61

Table S2: heart looping defects in std-MO and adap2-MO injected embryos at 2 dpf as shown by cmlc2 expression pattern analysis (Figure 4). n. = total number of injected embryos.

		Heart loop (%)				
Injected morpholino	**n.**	D-loop	Reduced loop	No loop	Reversed loop	Total heart looping defects
std-MO	53	96	0	4	0	4
adap2-MO	49	22	18	47	12	77

Table S3: Primers Used to Generate the Probes for Whole-Mount *In Situ* Hybridization Experiments.

Name	**Sequence (5'-3')**	**Tm**
Adap2P_fw	CTCGTGCCTCTCATCACCAG	64°C
Adap2P_rev	CCAGTGTAGTCCAGGTTGTC	62°C
Suz12P_fw	AGCATAATGTCAATAGATAAAGC	60°C
Suz12P_rev	CATCTTCTGAATCTCCAACTG	60°C
Utp6P_fw	GCTCCAGGTGCTCATTGACTC	66°C
Utp6P_rev	GGTTGAGGCAGTCCATCCAC	64°C
adap2P_fw	CTTTCCAACTGCTAGTGATGTAG	66°C
adap2P_rev	CGCCAGACAGAGACAAGACTC	66°C